

The Eclipsing δ Scuti Star EPIC 245932119

Jae Woo Lee^{1,2}, Kyeonsoo Hong^{1,3}, and Martti H. Kristiansen^{4,5}

¹*Korea Astronomy and Space Science Institute, Daejeon 34055, Korea*

²*Astronomy and Space Science Major, Korea University of Science and Technology, Daejeon 34113, Korea*

³*Institute for Astrophysics, Chungbuk National University, Cheongju 28644, Korea*

⁴*DTU Space, National Space Institute, Technical University of Denmark, Elektrovej 327, DK-2800 Lyngby, Denmark*

⁵*Brorfelde Observatory, Observator Gyldenkernes Vej 7, DK-4340 Tølløse, Denmark*

jwlee@kasi.re.kr

ABSTRACT

We present the physical properties of EPIC 245932119 ($K_p = +9.82$) exhibiting both eclipses and pulsations from the *K2* photometry. The binary modeling indicates that the eclipsing system is in detached or semi-detached configurations with a mass ratio of 0.283 or 0.245, respectively, and that its light-curve parameters are almost unaffected by pulsations. Multiple frequency analyses were performed for the light residuals in the outside-primary eclipsing phase after subtracting the binarity effects from the observed data. We detected 35 frequencies with signal to noise amplitude ratios larger than 4.0 in two regions of $0.62\text{--}6.28\text{ day}^{-1}$ and $19.36\text{--}24.07\text{ day}^{-1}$. Among these, it is possible that some high signals close to the Nyquist limit f_{Ny} may be reflections of real pulsation frequencies ($2f_{\text{Ny}} - f_i$). All frequencies ($f_8, f_9, f_{14}, f_{18}, f_{24}, f_{32}$) in the lower frequency region are orbital harmonics, and three high frequencies (f_{19}, f_{20}, f_{22}) appear to be sidelobes split from the main frequency of $f_1 = 22.77503\text{ day}^{-1}$. Most of them are thought to be alias effects caused by the orbital frequency. For the 26 other frequencies, the pulsation periods and pulsation constants are in the ranges of $0.041\text{--}0.052\text{ days}$ and $0.013\text{--}0.016\text{ days}$, respectively. These values and the position in the Hertzsprung-Russell diagram reveal that the primary component is a δ Sct pulsator. The observational properties of EPIC 245932119 are in good agreement with those for eclipsing binaries with δ Sct-type pulsating components.

Subject headings: binaries: eclipsing — stars: fundamental parameters — stars: individual (EPIC 245932119) — stars: oscillations (including pulsations)

1. INTRODUCTION

For eclipsing binaries (EBs), it is possible to measure precisely and directly fundamental stellar parameters, such as mass, radius, and luminosity through time-series photometry and spectroscopy, while pulsating stars provide valuable information about their interior structure through asteroseismology. Thus, EBs with pulsating components are attractive objects that test stellar structure and evolution models from their binarity and pulsation features. Over 90 of them have been known to contain δ Sct-type pulsating components (Kahraman Aliçavuş et al. 2017; Liakos & Niarchos 2017). The δ Sct pulsations are low-order pressure (p) modes driven by the κ mechanism acting in the He II ionization region and assist in probing the envelope of a star. The δ Sct components in binaries have pulsation characteristics similar to single δ Sct stars, but their pulsations may be influenced by the binary effects, such as tidal interaction and mass transfer between both components. Recently, Liakos & Niarchos (2015, 2017) proposed that there is a threshold in the binary period of ~ 13 days below which the binarity affects the pulsation properties and there exists a linear correlation between orbital and pulsation periods. Kahraman Aliçavuş et al. (2017) compared the physical parameters of pulsating EBs with those of single pulsators and showed that the δ Sct components in EBs pulsate with shorter periods and lower amplitudes. However, most of the eclipsing δ Sct stars still have not been studied in detail because of the lack of observed data (Liakos & Niarchos 2017; Kahraman Aliçavuş et al. 2017).

This paper is the seventh contribution in a series of detailed studies for the pulsating EBs using the precise photometric data from the space missions (Lee et al. 2014, 2016a,b, 2017; Lee 2016; Lee & Park 2018). We choose the *K2* target EPIC 245932119 (HD 220687, ASAS J232548-1136.6, RAVE J232547.8-113636, TYC 5825-1038-1; $K_p = +9.820$; $V_T = +9.622$, $(B - V)_T = +0.201$) with the *Kepler* spacecraft (Koch et al. 2010). From the All Sky Automated Survey (ASAS)-3 database, Pigulski & Michalska (2007) claimed that the stellar system is a pulsating EB with an orbital period of 1.594251 ± 0.000003 days and a dominant frequency of 26.16925 ± 0.00004 days $^{-1}$, corresponding to a pulsation period of about 0.03821 days. Wraight et al. (2011) identified the variability of this star as an EB with a period of 1.59430 days and a primary eclipse depth of 0.15 mag using the STEREO observations (Kaiser et al. 2008). On the other hand, Gray et al. (2017) conducted a survey in the southern hemisphere to increase the number of λ Boo stars, which are a rare class of Population I metal-weak A-type stars. They reported that the infrared excesses detected in EPIC 245932119 are not the λ Boo phenomena but arise from the presence of the cooler component.

Our results from both the binary modeling and the pulsation analysis indicate that EPIC 245932119 is a short-period EB with a δ Sct-type pulsating component. This study follows the following structure. In section 2, we present the light-curve synthesis for the observed *K2* data with an extensive mass-ratio (q) search. Section 3 describes the multiple frequency analyses for the eclipse-subtracted light residuals, using the iteration method applied in a paper of Lee et al. (2017). Finally, the discussion and conclusions for this work are given in section 4.

2. K2 PHOTOMETRY AND LIGHT-CURVE SYNTHESIS

EPIC 245932119 was observed in a long cadence mode with an integration time of 29.42 min during Campaign 12 of the *Kepler* K2 mission (Howell et al. 2014). We used the simple aperture photometry (SAP) data from the MAST Archive¹. The raw data were detrended by fitting the out-of-eclipse part of the orbital light curve to a straight line and were converted to a magnitude scale by requiring a *Kepler* magnitude of +9.82 at maximum light. As shown in Figure 1, the K2 light curve displays an ellipsoidal variation outside eclipses, which may be partly caused by tidal distortion. The depth difference between the primary and secondary eclipses indicates a large temperature difference between both components. In order to obtain the light-curve parameters of the binary star, we analyzed the K2 data using the 2007 version of the Wilson-Devinney synthesis code (Wilson & Devinney 1971, van Hamme & Wilson 2007; hereafter W-D).

The light-curve modeling of our program target was done in a manner similar to that for the pulsating EBs KIC 6220497 (Lee et al. 2016a) and KIC 11401845 (Lee et al. 2017). The surface temperature of the hotter primary component was set to be $T_1 = 7,652 \pm 95$ K from the RAVE (RAAdial Velocity Experiment; Kordopatis et al. 2013) Catalogue. The logarithmic bolometric ($X_{1,2}$) and monochromatic ($x_{1,2}$) limb-darkening coefficients were interpolated from the tables of van Hamme (1993). The gravity-darkening exponents ($g_{1,2}$) and the bolometric albedos ($A_{1,2}$) were held fixed at standard values of $g_1 = 1.0$ and $g_2 = 0.32$, and $A_1 = 1.0$ and $A_2 = 0.5$, as surmised from the components’ temperatures. In Figure 1, the secondary eclipses are consistent with one half period after the primary eclipses, which implies that EPIC 245932119 has negligible eccentricity. As expected for short-period binaries, a synchronous rotation for both components ($F_{1,2} = 1.0$) was adopted, and the detailed reflection treatment was applied. It is known that the F values cause little impact on the light-curve parameters (e.g., Lee et al. 2018). In this paper, the adjustable parameters were the orbital ephemeris (T_0 and P), the inclination angle (i), the temperature (T_2) of the secondary star, the dimensionless surface potential ($\Omega_{1,2}$), and the monochromatic luminosity (L_1).

The mass ratio (q) is one of the most important parameters in studying the Roche-geometry configuration and physical properties of EBs. Nonetheless, neither light-curve solution nor spectroscopic q have been made for EPIC 245932119. Thus, we conducted the so-called q -search procedure that computes a series of models with varying q for various modes of the W-D code. The behavior of the weighted sum of the squared residuals ($\sum W(O - C)^2$; hereafter Σ) was used to estimate the potential reality of each model. The results are displayed in Figure 2, and we found two possible Roche geometries: a detached configuration with $q = 0.28$ and a semi-detached configuration (the secondary component filling its limiting lobe) with $q = 0.24$. In the subsequent calculations, the q values were used as an additional free parameter in each configuration to derive the binary parameters listed in Table 1. The photometric solution for the detached mode appears as a blue solid curve

¹<http://archive.stsci.edu/k2/>

in the top panel of Figure 3, and the corresponding light residuals are plotted in the middle panel of the figure. The semi-detached mode also led to the same results. In all procedures, we included the orbital eccentricity as an adjustable parameter, but its value remained indistinguishable from zero. This indicates that our program target is in a circular orbit.

3. LIGHT-CURVE RESIDUALS AND PULSATIONAL CHARACTERISTICS

From its temperature, the primary star of EPIC 245932119 would be a candidate for δ Sct and/or γ Dor pulsators. Pigulski & Michalska (2007) reported that the EB system is pulsating at frequencies of $f_{PM_1} = 26.16925 \text{ days}^{-1}$ and possibly $f_{PM_2} = 23.0413 \text{ days}^{-1}$. So then, the pulsations can be attributed to δ Sct-type variability. In order to search for more reliable pulsation frequencies in the binary star, we followed an approach analogous to that of Lee et al. (2017). First of all, we made a total of 46 light curves at intervals of one orbital period and separately analyzed them for the detached and semi-detached modes by adjusting only the reference epoch (T_0) among the photometric parameters in Table 1. Then, we performed a multiple frequency analysis for the corresponding light residuals in the outside-primary eclipsing phase. The PERIOD04 program (Lenz & Breger 2005) was carried out in the frequency range from 0 to the Nyquist limit of $f_{Ny} = 24.47 \text{ days}^{-1}$. After the successive prewhitening of each frequency peak (see Lee et al. 2014), we detected the frequencies based on the empirical threshold of the signal to noise amplitude ratio (S/N) larger than 4.0 (Breger et al. 1993). Third, we removed the pulsation signatures from the observed *K2* data. The pulsation-subtracted data were modeled using the W-D code, and the new light-curve parameters were used to reanalyze the 46 light curves in the first step.

This procedure was iterated 7 and 5 times, respectively, for the detached and semi-detached modes until both detected frequencies and binary parameters were unchanged. The physical parameters of EPIC 245932119 are given in Table 2, and the pulsation-subtracted data and synthetic light curve for the detached mode are illustrated in the top panel of Figure 3. In Tables 1 and 2, the binary parameters from the observed and pulsation-subtracted data are in good agreement with each other. The light residuals after removing the binary effects from the observed data for the detached mode are plotted in Figure 4 as magnitude versus BJD, where the lower panel presents a short section of the residuals. As the result of our detailed analyses, we found 35 frequencies with the criterion of $S/N > 4.0$. The periodogram from the PERIOD04 program is shown in Figure 5. The spectral window in the first panel shows strong side bands at integer multiples of the orbital frequency ($f_{orb} = 0.62727 \text{ days}^{-1}$), which may be produced by excluding the data of the primary eclipses. The amplitude spectra for EPIC 245932119 before and after prewhitening the first 7 frequencies and then all 35 frequencies are shown in the second to bottom panels of Figure 5, respectively. The results are listed in Table 3, wherein the uncertainties were calculated according to Kallinger et al. (2008). The synthetic curve calculated from the 35-frequency fit is displayed in the lower panel of Figure 4.

As shown in Figure 5 and Table 3, the main signals of EPIC 245932119 lie in two frequency

regions of $< 7 \text{ days}^{-1}$ and $> 19 \text{ days}^{-1}$. Within the frequency resolution of $1.5/\Delta T = 0.019 \text{ days}^{-1}$ (ΔT is the time base of observations; Loumos & Deeming 1978), we searched for possible harmonic and combination frequencies. As a consequence, the six frequencies ($f_8, f_9, f_{14}, f_{18}, f_{24}, f_{32}$) in the low frequency region are the orbital frequency of f_{orb} and its multiples, which can be partially attributed to imperfect removal of the binary effects from the observed data. Further, f_{19}, f_{20} , and f_{22} appear to be the sidelobes split from the f_1 frequency by f_{orb} . On the other hand, some frequencies near the Nyquist limit f_{Ny} can be reflections of real pulsations ($2f_{\text{Ny}} - f_i$) higher than f_{Ny} (Murphy et al. 2013; Lee et al. 2016b). It is possible that our frequency of $f_1 = 22.77503 \text{ days}^{-1}$ may be a reflection ($2f_{\text{Ny}} - f_{\text{PM}_1} = 22.77075 \text{ days}^{-1}$) of a signal detected by Pigulski & Michalska (2007). However, at present, we find it difficult to distinguish real peaks from the Nyquist aliases.

4. DISCUSSION AND CONCLUSIONS

In this paper, we have studied both binarity and pulsation of EPIC 245932119 from the *K2* data made during the Campaign 12. The binary light curve was satisfactorily analyzed for two cases: including and removing oscillation frequencies. The results indicate that the EB system is in a detached configuration with $q = 0.283$ or a semi-detached configuration with $q = 0.245$, and that its binary parameters are not affected by the pulsations. In the detached mode, both components fill $F_1 = 77 \%$ and $F_2 = 93 \%$ of their inner critical lobe, respectively, while $F_1 = 73 \%$ in the semi-detached mode. Here, the fill-out factor $F_{1,2} = \Omega_{\text{in}}/\Omega_{1,2}$, where Ω_{in} is the potential of the inner Roche surface. There is currently no way to know which Roche configuration is more appropriate to describe our program target.

The effective temperature of the primary component corresponds to a normal main-sequence star with a spectral type of about A7V (Harmanec 1988; Pecaut & Mamajek 2013). Based on the empirical relation between spectral type and stellar mass, we estimated the primary’s mass to be $M_1 = 1.75 \pm 0.18 M_{\odot}$ with an error of 10 % assumed. Then, the absolute dimensions of EPIC 245932119 were computed from the light-curve parameters and the M_1 value, and they are listed in the bottom of Table 2. We calculated the luminosity (L) and bolometric magnitudes (M_{bol}) by using $T_{\text{eff}\odot} = 5,780 \text{ K}$ and $M_{\text{bol}\odot} = +4.73$ for solar values. The bolometric corrections (BCs) were derived from the expression between $\log T_{\text{eff}}$ and BC (Torres 2010). Using the estimated parameters, we examined the evolutionary state of EPIC 245932119 in mass-radius, mass-luminosity, and Hertzsprung-Russell (HR) diagrams (İbanoğlu et al. 2006; Lee & Park 2018). In these diagrams, the pulsating primary star resides within the δ Sct instability strip on the main-sequence band, while the low-mass companion is remarkably larger and brighter than expected for main-sequence stars of the same mass. This indicates that the secondary component is highly evolved.

With an apparent visual magnitude of $V = +9.604 \pm 0.035$ (Høg et al. 2000) and the interstellar reddening of $A_V = 0.100$ (Schlafly & Finkbeiner 2011), we determined the distance of our program target to be $429 \pm 23 \text{ pc}$ and $412 \pm 22 \text{ pc}$, respectively, for the detached and semi-

detached modes. Considering that the physical properties of EPIC 245932119 were obtained from the mass-spectral type relation without the radial velocities of each component, these values are in satisfactory agreement with the Gaia distance of 463 ± 11 pc computed from Gaia DR2² (2.16 ± 0.05 mas; Gaia Collaboration et al. 2018). On this account, it is not possible to distinguish between the two Roche modes from the distance determination.

In order to investigate the pulsational characteristics of EPIC 245932119, multiple frequency analyses were applied to the light-curve residuals in the out-of-primary eclipsing phase after removing the binarity effects from the observed data. As a result, we found the 35 frequencies with S/N larger than 4.0 in two ranges of $0.62\text{--}6.28$ days⁻¹ and $19.36\text{--}24.07$ days⁻¹. Among these, nine frequencies are orbital harmonics ($f_8, f_9, f_{14}, f_{18}, f_{24}, f_{32}$) and combination terms (f_{19}, f_{20}, f_{22}), most of which may arise from alias effects caused by the orbital frequency. Applying the absolute parameters in the detached mode of Table 2 to the well-known relation of $\log Q_i = -\log f_i + 0.5 \log g + 0.1 M_{\text{bol}} + \log T_{\text{eff}} - 6.456$ (Petersen & Jørgensen 1972), we computed the pulsation constants for the remaining 26 frequencies, and they are given in the sixth column of Table 3. The Q values of $0.013\text{--}0.016$ days and the pulsation periods (P_{pul}) of $0.041\text{--}0.052$ days correspond to the low-order pressure modes of δ Sct pulsators with the typical ranges of $Q < 0.04$ days and $P_{\text{pul}} = 0.02\text{--}0.2$ days (Breger 2000). Moreover, as mentioned above, the primary component lies inside the δ Sct region of the HR diagram. The results demonstrate that EPIC 245932119 is an EB system with a δ Sct-type pulsating component. The binary parameters in Table 2, the pulsation quantities in Table 3, and the gravitational force of $\log(F/M_1) = 2.76$ (that is applied to the pulsating primary by its companion) match well empirical relations of the δ Sct pulsators in binaries (Kahraman Alıçavuş et al. 2017; Liakos & Niarchos 2017).

Because EPIC 245932119 is bright enough for spectroscopic follow-up or other observations, future high-resolution spectra will assist in measuring the double-lined radial velocities and spectroscopic mass ratio and hence in determining its Roche configuration and absolute parameters. High-cadence multi-band photometry is needed to identify the detected frequencies and pulsation modes of the EB system. These offer us an important piece of observational evidence for studying the interesting objects.

This paper includes data collected by the *K2* mission. Funding for the *K2* mission is provided by the NASA Science Mission directorate. Some of the data presented in this paper were obtained from the Mikulski Archive for Space Telescopes (MAST). We appreciate the careful reading and valuable comments of the anonymous referee. This research has made use of the Simbad database maintained at CDS, Strasbourg, France, and was supported by the KASI grant 2018-1-830-02. K.H. was supported by the grant numbers 2017R1A4A1015178 of the National Research Foundation (NRF) of Korea. M.H.K. acknowledges Allan R. Schmitt for making the LcTools software.

²<https://gea.esac.esa.int/archive/>

REFERENCES

- Breger, M. 2000, in ASP Conf. Ser. 210, Delta Scuti and Related Stars, ed. M. Breger, & M. H. Montgomery (San Francisco: ASP), 3
- Breger, M., Stich, J., Garrido, R., et al. 1993, *A&A*, 271, 482
- Gaia Collaboration, Brown, A. G. A., Vallenari, A., et al. 2018, *A&A*, 616, A1
- Gray, R. O., Riggs, Q. S., Koen, C., et al. 2017, *AJ*, 154, 31
- Harmanec, P. 1988, *Bull. Astron. Inst. Czechoslovakia*, 39, 329
- Høg, E., Fabricius, C., Makarov, V. V., et al. 2000, *A&A*, 355, 27
- Howell, S. B., Sobeck, C., Haas, M., et al. 2014, *PASP*, 126, 398
- İbanoğlu, C., Soyduğan, F., Soyduğan, E., & Dervişoğlu, A. 2006, *MNRAS*, 373, 435
- Kahraman Aliçavuş, F., Soyduğan, E., Smalley, B., & Kubát, J. 2017, *MNRAS*, 470, 915
- Kaiser, M. L., Kucera, T. A., Davila, J. M., et al. 2008, *SSRv*, 136, 5
- Kallinger, T., Reegen, P., & Weiss, W. W. 2008, *A&A*, 481, 571
- Koch, D. G., et al. 2010, *ApJ*, 713, L79
- Kordopatis, G., Gilmore, G., Steinmetz, M., et al. 2013, *AJ*, 146, 134
- Lee, J. W. 2016, *ApJ*, 833, 170
- Lee, J. W., Hong, K., Kim, S.-L., & Koo, J.-R. 2016a, *MNRAS*, 460, 4220
- Lee, J. W., Hong, K., Kim, S.-L., & Koo, J.-R. 2017, *ApJ*, 835, 189
- Lee, J.-W., Hong, K., Koo, J.-R., & Park, J.-H. 2018, *AJ*, 155, 5
- Lee, J. W., Kim, S.-L., Hong, K., Koo, J.-R., Lee, C.-U., & Youn, J.-H. 2016b, *AJ*, 151, 25
- Lee, J. W., Kim, S.-L., Hong, K., Lee, C.-U., & Koo, J.-R. 2014, *AJ*, 148, 37
- Lee, J. W., & Park, J.-H. 2018, *MNRAS*, 480, 4693
- Lenz, P., & Breger, M. 2005, *Comm. Asteroseismology*, 146, 53
- Liakos, A., & Niarchos, P. 2015, in ASP Conf. Ser. 496, ed. S. M. Rucinski, G. Torres, & M. Zejda (San Francisco: ASP), 195
- Liakos, A., & Niarchos, P. 2017, *MNRAS*, 465, 1181

- Loumos, G. L., & Deeming, T. J. 1978, *Ap&SS*, 56, 285
- Murphy, S. J., Shibahashi, H., & Kurtz, D. W., 2013, *MNRAS*, 430, 2986
- Pecaut, M. J., & Mamajek, E. E. 2013, *ApJS*, 208, 9
- Petersen, J. O., & Jørgensen, H. E. 1972, *A&A*, 17, 367
- Pigulski, A., & Michalska, G. 2007, *AcA*, 57, 61
- Schlafly, E. F., & Finkbeiner, D. P. 2011, *AJ*, 737, 103
- Torres, G. 2010, *AJ*, 140, 1158
- Van Hamme, W. 1993, *AJ*, 106, 209
- Van Hamme, W., & Wilson, R. E. 2007, *ApJ*, 661, 1129
- Wilson, R. E., & Devinney, E. J. 1971, *ApJ*, 166, 605
- Wraight, K. T., White, G. J., Bewsher, D., & Norton, A. J. 2011, *MNRAS*, 416, 2477

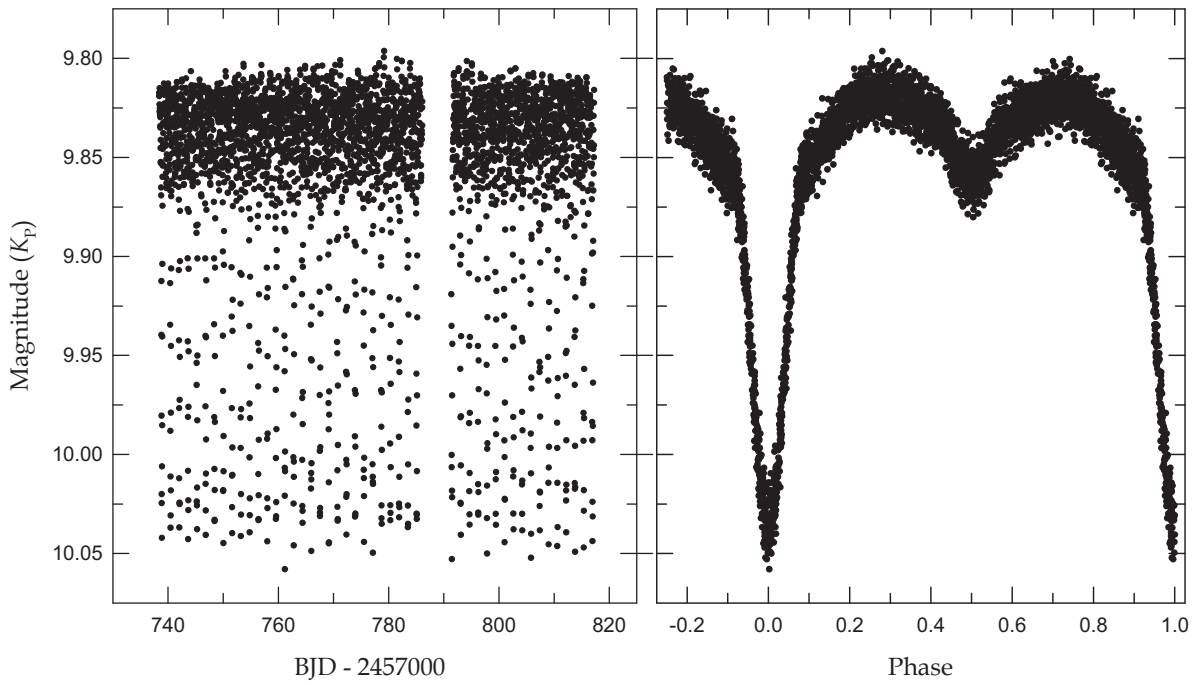


Fig. 1.— *K2* observations of EPIC 245932119 distributed in BJD (left panel) and orbital phase (right panel).

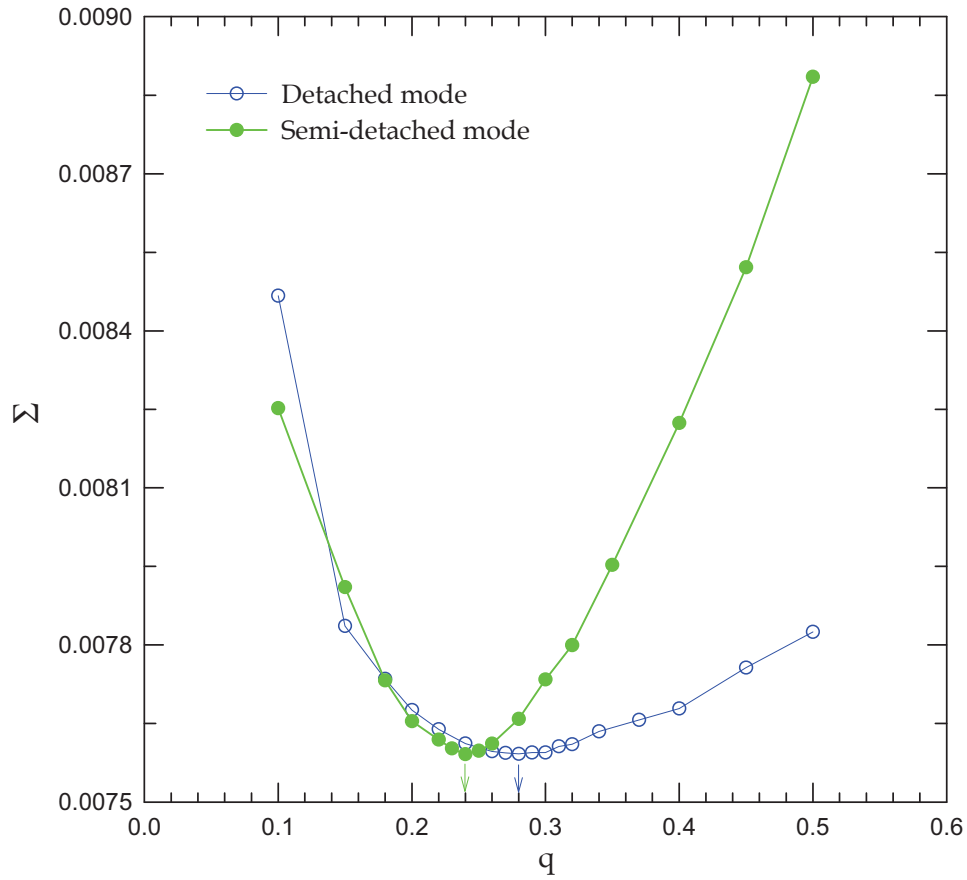


Fig. 2.— Behavior of Σ (the weighted sum of the residuals squared) as a function of the mass ratio q . The open and filled circles represent the q -search results for the detached and semi-detached configurations, respectively.

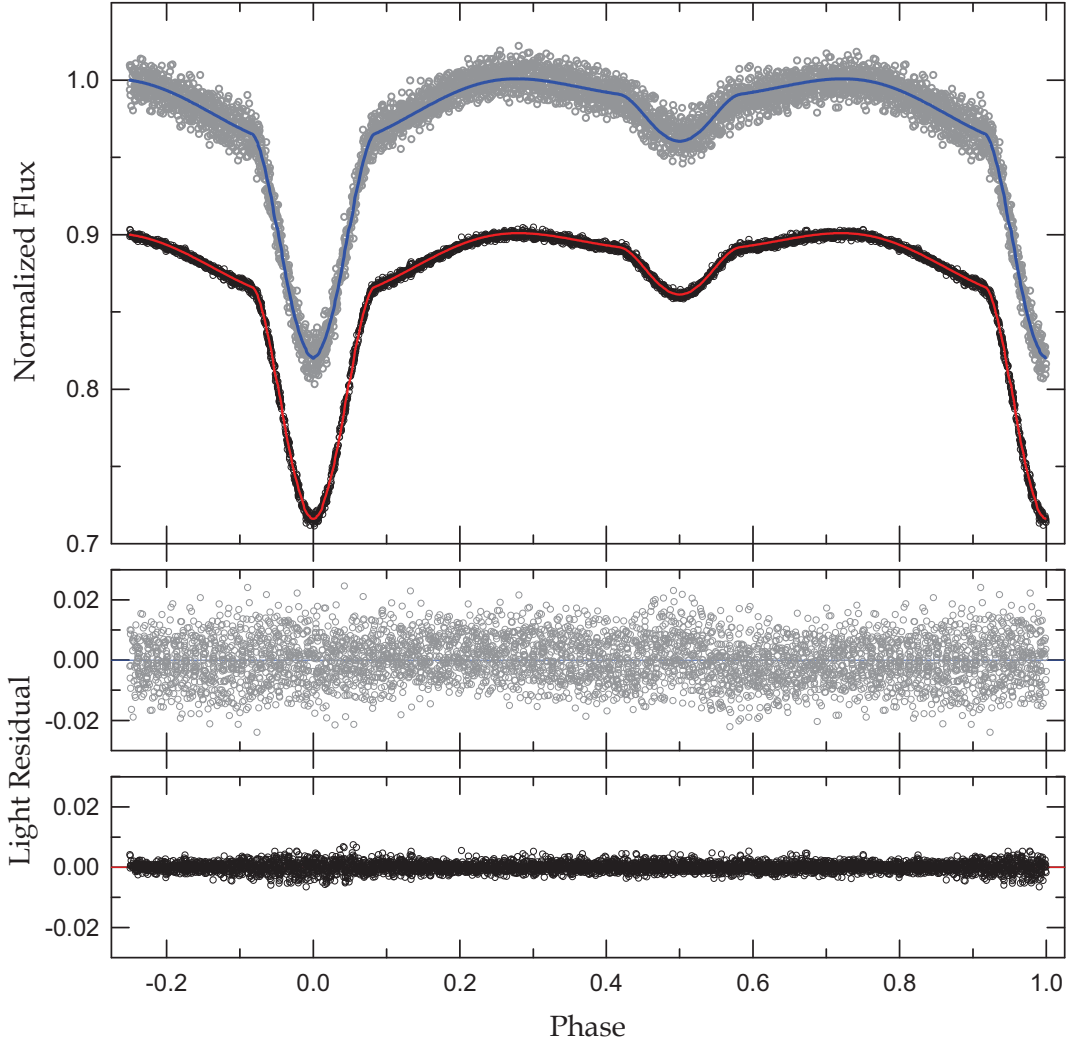


Fig. 3.— Binary light curve before (gray circle) and after (black circle) subtracting the pulsation signatures from the observed *K2* data. The blue and red solid curves are computed with the photometric solutions for the detached modes in Tables 1 and 2, respectively. The corresponding residuals from the fits are plotted at the middle and bottom panels in the same order as the light curves.

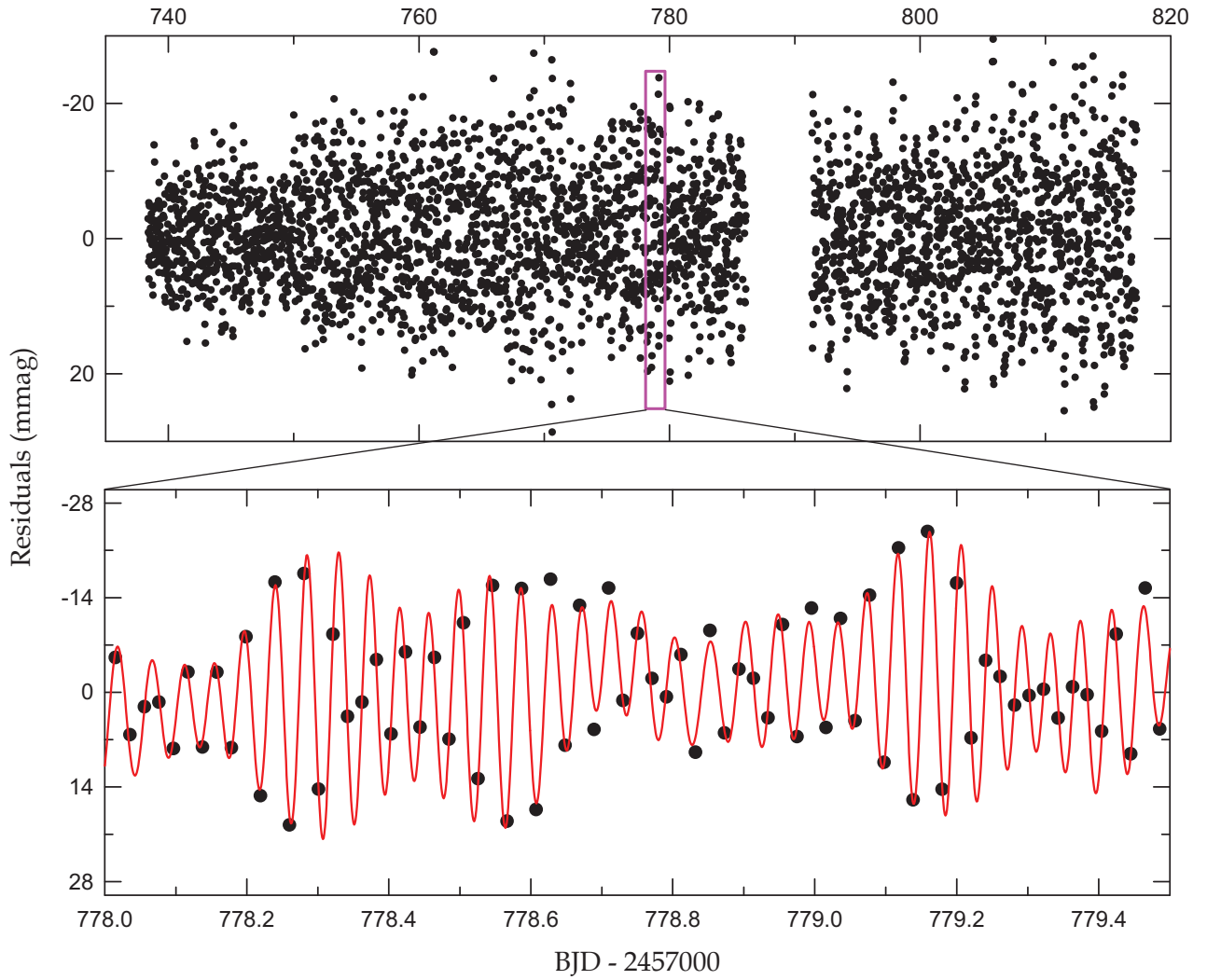


Fig. 4.— Light-curve residuals after removing the binarity effects from the observed data. The lower panel presents a short section of the residuals marked by the inset box in the upper panel. The synthetic curve is computed from the 35-frequency fit to the data.

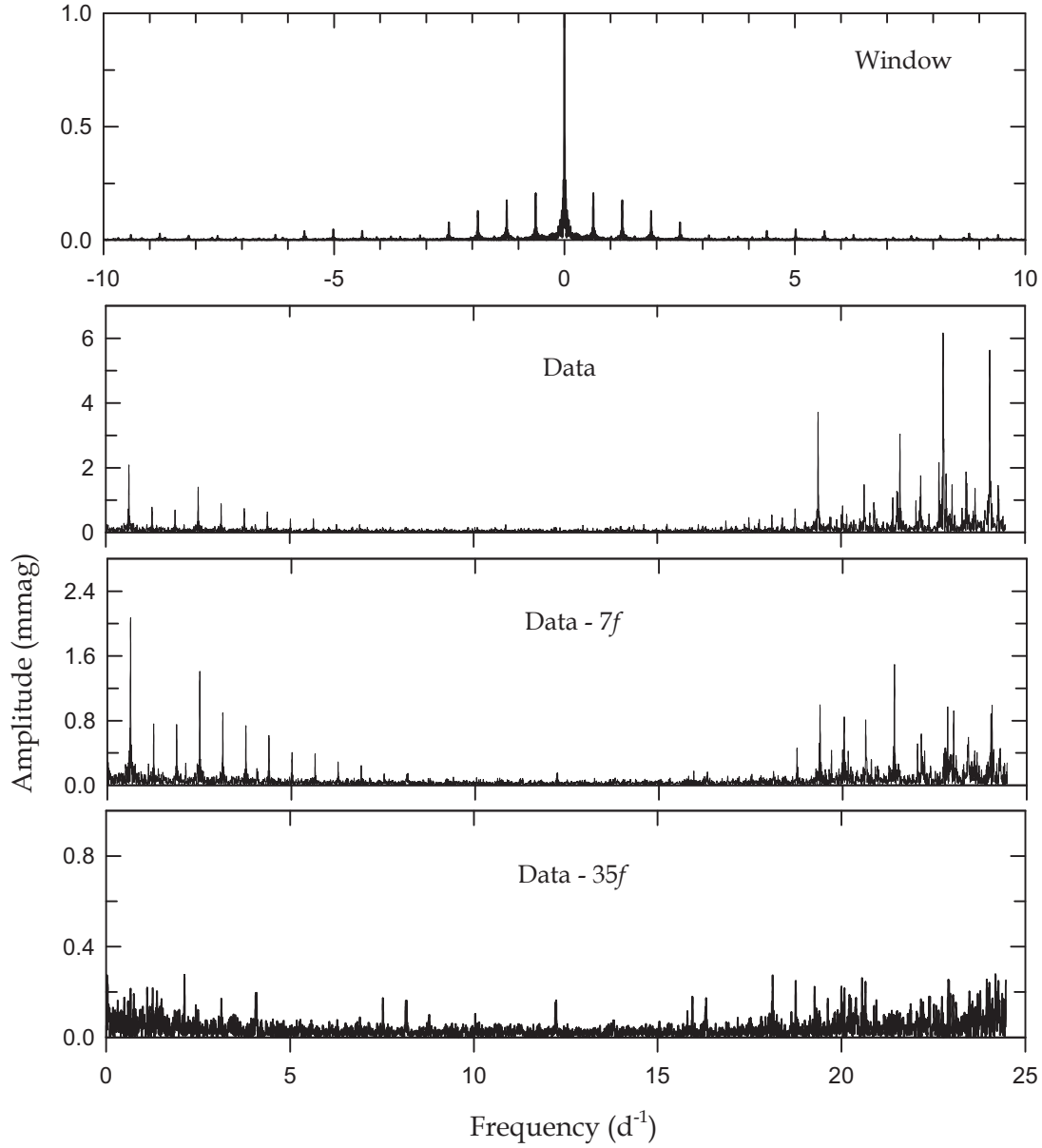


Fig. 5.— Periodogram from the PERIOD04 program for the entire light residuals in the out-of-primary eclipsing phase ($0.09-0.91P$). The window spectrum is displayed in the top panel. The amplitude spectra before and after prewhitening the first 7 frequencies and all 35 frequencies are shown in the second to bottom panels.

Table 1. Binary Parameters of EPIC 245932119 from the Observed Data

Parameter	Detached Mode		Semi-detached Mode	
	Primary	Secondary	Primary	Secondary
T_0 (BJD)	2,457,773.92915(35)		2,457,773.92896(35)	
P (day)	1.594195(23)		1.594197(23)	
q	0.2810(13)		0.2411(15)	
i (deg)	68.31(33)		66.74(12)	
T (K)	7652(95)	3824(41)	7652(95)	4038(34)
Ω	3.119(13)	2.600(22)	3.180(26)	2.332
Ω_{in}	2.424		2.332	
A	1.0	0.5	1.0	0.5
g	1.0	0.32	1.0	0.32
X, Y	0.672, 0.200	0.611, 0.156	0.672, 0.200	0.617, 0.151
x, y	0.597, 0.239	0.745, 0.033	0.597, 0.239	0.754, 0.043
$L/(L_1+L_2)$	0.9837(26)	0.0163	0.9644(26)	0.0356
r (pole)	0.3505(17)	0.2223(37)	0.3388(45)	0.2456(5)
r (point)	0.3722(23)	0.2521(66)	0.3554(56)	0.3585(6)
r (side)	0.3609(20)	0.2281(42)	0.3475(50)	0.2556(5)
r (back)	0.3672(21)	0.2434(54)	0.3521(53)	0.2882(5)
r (volume) ^a	0.3597(20)	0.2315(49)	0.3462(51)	0.2640(5)
$\sum W(O - C)^2$	0.00756		0.00756	

^aMean volume radius.

Table 2. Binary Parameters of EPIC 245932119 from the Pulsation-Subtracted Data

Parameter	Detached Mode		Semi-detached Mode	
	Primary	Secondary	Primary	Secondary
T_0 (BJD)	2,457,773.929462(70)		2,457,773.929566(73)	
P (day)	1.5941988(47)		1.5942005(49)	
q	0.2825(13)		0.2450(16)	
i (deg)	68.69(13)		66.75(7)	
T (K)	7652(95)	3834(30)	7652(95)	4039(12)
Ω	3.155(16)	2.609(8)	3.212(19)	2.341
Ω_{in}	2.427		2.341	
X, Y	0.672, 0.200	0.611, 0.156	0.672, 0.200	0.617, 0.151
x, y	0.597, 0.239	0.746, 0.035	0.597, 0.239	0.754, 0.043
$L/(L_1+L_2)$	0.9829(10)	0.0171	0.9633(10)	0.0367
r (pole)	0.3462(19)	0.2218(22)	0.3356(23)	0.2468(5)
r (point)	0.3667(25)	0.2510(37)	0.3517(29)	0.3601(6)
r (side)	0.3561(22)	0.2275(24)	0.3440(26)	0.2568(5)
r (back)	0.3621(24)	0.2425(30)	0.3485(27)	0.2894(5)
r (volume)	0.3550(22)	0.2309(28)	0.3428(26)	0.2652(5)
$\sum W(O - C)^2$	0.00153		0.00155	
Absolute parameters:				
M (M_\odot)	1.75(18)	0.49(5)	1.75(18)	0.43(4)
R (R_\odot)	2.67(12)	1.73(8)	2.55(11)	1.97(9)
$\log g$ (cgs)	3.83(6)	3.65(6)	3.87(6)	3.48(6)
L (L_\odot)	22(2)	0.58(6)	20(2)	0.93(8)
M_{bol} (mag)	1.38(11)	5.32(11)	1.48(11)	4.81(10)
BC (mag)	0.03(1)	-1.41(6)	0.03(1)	-1.07(2)
M_V (mag)	1.35(11)	6.73(12)	1.45(11)	5.88(10)
Distance (pc)	429 \pm 23		412 \pm 22	

Table 3. Multiple Frequency Analysis of EPIC 245932119^a

	Frequency (day ⁻¹)	Amplitude (mmag)	Phase (rad)	S/N ^b	<i>Q</i> (days)	Remark
f_1	22.77503±0.00005	6.42±0.12	1.94±0.06	88.62	0.013	
f_2	24.04266±0.00005	5.86±0.13	0.42±0.06	78.88	0.013	
f_3	19.37332±0.00006	3.43±0.08	2.79±0.07	70.71	0.016	
f_4	22.79150±0.00009	3.62±0.12	0.30±0.10	49.92	0.013	
f_5	21.60056±0.00010	2.71±0.11	3.93±0.12	42.91	0.014	
f_6	24.05154±0.00010	3.24±0.13	5.07±0.11	43.64	0.013	
f_7	22.66157±0.00013	2.40±0.12	1.24±0.15	33.22	0.013	
f_8	0.62685±0.00013	2.09±0.11	5.88±0.16	32.22		f_{orb}
f_9	2.50992±0.00013	1.78±0.09	5.84±0.15	33.81		$4f_{\text{orb}}$
f_{10}	21.40661±0.00017	1.55±0.10	0.74±0.20	25.67	0.014	
f_{11}	19.38409±0.00022	0.96±0.08	1.52±0.25	19.66	0.016	
f_{12}	24.06168±0.00032	1.00±0.13	4.43±0.38	13.35	0.013	
f_{13}	22.85552±0.00031	1.00±0.12	1.24±0.36	13.76	0.013	
f_{14}	3.76425±0.00015	1.18±0.07	5.06±0.17	28.75		$6f_{\text{orb}}$
f_{15}	23.01905±0.00035	0.90±0.13	0.96±0.41	12.20	0.013	
f_{16}	20.04010±0.00028	0.82±0.09	5.20±0.32	15.49	0.015	
f_{17}	20.62638±0.00029	0.84±0.10	2.43±0.34	14.87	0.015	
f_{18}	5.01858±0.00018	0.79±0.06	4.20±0.21	23.92		$8f_{\text{orb}}$
f_{19}	22.13804±0.00049	0.61±0.12	2.78±0.56	8.90		$f_1 - f_{\text{orb}}$
f_{20}	23.41835±0.00041	0.77±0.12	2.49±0.47	10.60		$f_1 + f_{\text{orb}}$
f_{21}	24.03189±0.00043	0.75±0.13	3.79±0.50	10.11	0.013	
f_{22}	23.40060±0.00046	0.68±0.12	3.95±0.53	9.37		$f_1 + f_{\text{orb}}$
f_{23}	22.78326±0.00040	0.79±0.12	3.93±0.46	10.89	0.013	
f_{24}	6.27291±0.00029	0.46±0.05	3.41±0.33	15.09		$10f_{\text{orb}}$
f_{25}	19.69403±0.00051	0.43±0.09	1.87±0.59	8.43	0.015	
f_{26}	23.58885±0.00073	0.44±0.13	6.14±0.85	5.91	0.013	
f_{27}	23.08496±0.00076	0.41±0.12	3.54±0.88	5.69	0.013	
f_{28}	22.93602±0.00082	0.38±0.12	3.98±0.95	5.27	0.013	
f_{29}	23.50772±0.00080	0.39±0.12	1.51±0.93	5.38	0.013	
f_{30}	23.44814±0.00068	0.46±0.12	5.59±0.79	6.38	0.013	
f_{31}	22.81622±0.00072	0.43±0.12	5.59±0.84	5.96	0.013	
f_{32}	0.63509±0.00076	0.37±0.11	2.40±0.88	5.70		f_{orb}
f_{33}	23.91844±0.00094	0.34±0.13	0.23±1.09	4.61	0.013	
f_{34}	19.36318±0.00058	0.36±0.08	5.81±0.67	7.47	0.016	
f_{35}	22.74840±0.00097	0.32±0.12	4.56±1.13	4.43	0.013	

^aFrequencies are listed in order of detection.

^bCalculated in a range of 5 d^{-1} around each frequency.